The shared role of the Rsr1 GTPase and Gic1/Gic2 in Cdc42 polarization

Pil Jung Kang[a], Kristi E. Miller[b], Julia Guegueniat[a,†], Laure Beven[a,‡], and Hay-Oak Park[a,b,*]
[a]Department of Molecular Genetics and [b]Molecular Cellular Developmental Biology Program, The Ohio State University, Columbus, OH 43210

ABSTRACT **The Cdc42 GTPase plays a central role in polarity development in many species. In budding yeast, Cdc42 is essential for polarized growth at the proper site and also for spontaneous cell polarization in the absence of spatial cues. Cdc42 polarization is critical for multiple events in the G1 phase prior to bud emergence, including bud-site assembly, polarization of the actin cytoskeleton, and septin filament assembly to form a ring at the new bud site. Yet the mechanism by which Cdc42 polarizes is not fully understood. Here we report that biphasic Cdc42 polarization in the G1 phase is coupled to stepwise assembly of the septin ring for bud emergence. We show that the Rsr1 GTPase shares a partially redundant role with Gic1 and Gic2, two related Cdc42 effectors, in the first phase of Cdc42 polarization in haploid cells. We propose that the first phase of Cdc42 polarization is mediated by positive feedback loops that function in parallel—one involving Rsr1 via local activation of Cdc42 in response to spatial cues and another involving Gic1 or Gic2 via reduction of diffusion of active Cdc42.**

Monitoring Editor
Fred Chang
University of California, San Francisco

Received: Mar 5, 2018
Revised: Jul 11, 2018
Accepted: Jul 25, 2018

INTRODUCTION

Cell polarization often occurs along a single axis that is generally directed by extra- or intracellular cues. Cells of the budding yeast *Saccharomyces cerevisiae* are genetically programmed to undergo polarized growth by choosing a bud site, which determines the axis of polarized growth. Selection of a bud site depends on cell type: **a** and α cells (such as normal haploids) bud in the axial pattern, in which both mother and daughter cells select a new bud site adjacent to their immediately preceding division site. In contrast, **a**/α cells (such as normal diploids) form buds in the bipolar pattern, in which daughter cells bud preferentially at the pole distal to the division site, and mother cells can choose a bud site near either pole. The Rsr1 GTPase module, which consists of Rsr1 (also known as Bud1), its guanine nucleotide exchange factor (GEF) Bud5, and its GTPase activating protein (GAP) Bud2, functions in directing polarity establishment by guiding Cdc42 and its regulators in response to distinct cortical markers in each cell type (see references in Bi and Park, 2012).

In the absence of spatial cues, yeast cells can still polarize, albeit at a random site. This process, referred to as symmetry breaking, is thought to occur via positive feedback loops involving the scaffold protein Bem1 or the actin cytoskeleton, although several aspects of these mechanisms are under debate (see references in Martin [2015] and Goryachev and Leda [2017]). Cla4, a p21-activated protein kinase (PAK), is one of the Cdc42 effectors, which interact with Cdc42-GTP through the p21-binding domain (PBD), also known as Cdc42/Rac-interactive binding (CRIB) domain (Cvrckova *et al.*, 1995; Benton *et al.*, 1997). Cla4 is suggested to function with Bem1 and Cdc24, a Cdc42 GEF, in symmetry breaking (Kozubowski *et al.*, 2008). Gic1 and Gic2 also interact with Cdc42-GTP and are known to be involved in polarity establishment and septin organization (Brown *et al.*, 1997; Chen *et al.*, 1997; Bi *et al.*, 2000; Jaquenoud and Peter, 2000; Iwase *et al.*, 2006; Sadian *et al.*, 2013).

Despite substantial progress in deciphering the mechanisms underlying Cdc42 polarization, many questions remain. Of particular interest is how specific events during polarity establishment are coordinated with cell-cycle progression in G1, leading to bud

This article was published online ahead of print in MBoC in Press (http://www.molbiolcell.org/cgi/doi/10.1091/mbc.E18-02-0145) on August 9, 2018.

Present addresses: †Alberta RNA Research and Training Institute, Department of Chemistry and Biochemistry, University of Lethbridge, Lethbridge, AB T1K 3M4, Canada; ‡University of Bordeaux, INRA, UMR 1332, Fruit Biology and Pathology, Villenave d'Ornon 33882, France.

*Address correspondence to: Hay-Oak Park (park.294@osu.edu).

Abbreviations used: CRIB, Cdc42/Rac-interactive binding; FRAP, fluorescence recovery after photobleaching; GAP, GTPase-activating protein; GDI, guanine nucleotide dissociation inhibitor; GEF, guanine nucleotide exchange factor; GST, glutathione *S*-transferase; GTPase, guanosine triphosphatase; PBD, p21-binding domain; PM, plasma membrane; WT, wild type.

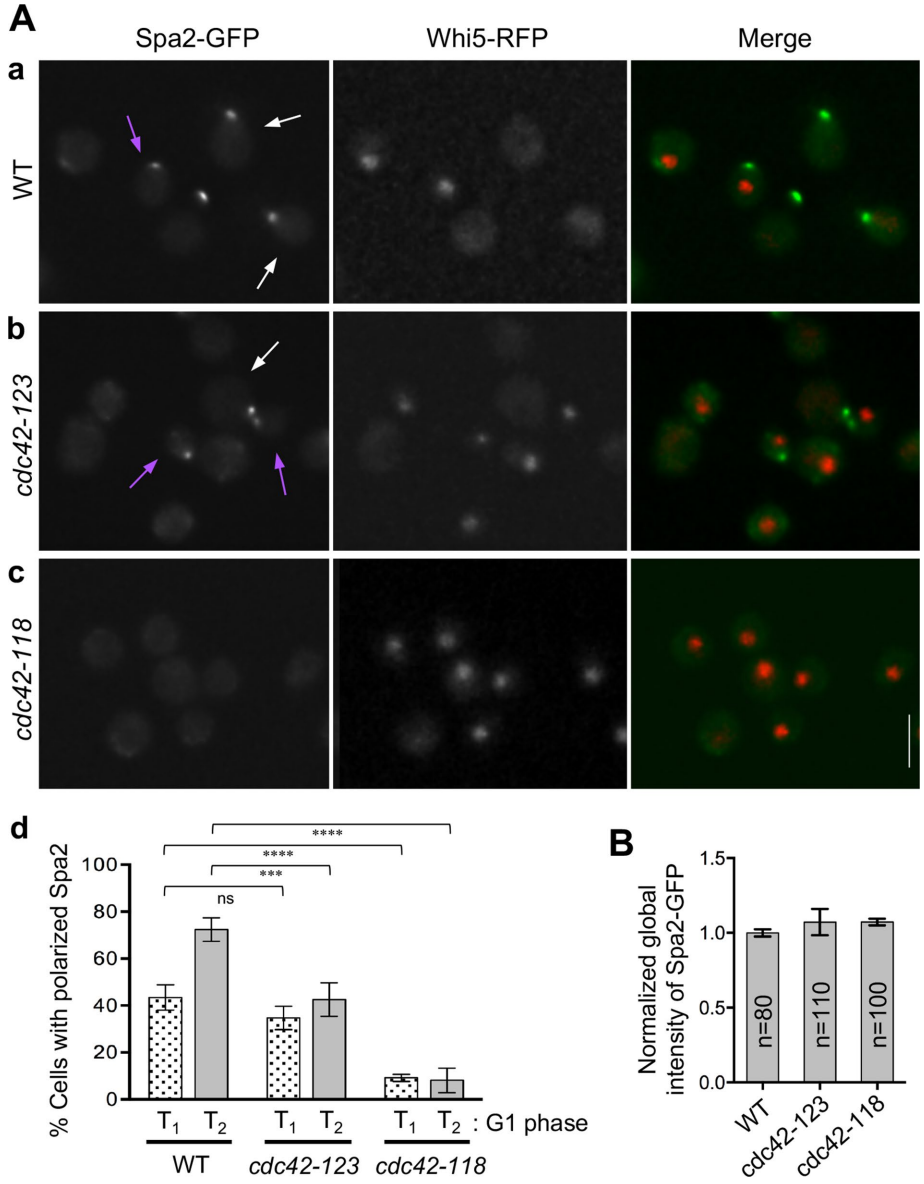

FIGURE 1: Localization of Spa2-GFP and Whi5-RFP in WT and *cdc42*^{ts} mutants at 37°C. (Aa-c) Representative images of each strain at 2 h after shifting to 37°C. Cells with polarized Spa1-GFP during the first (T_1) or second phase (T_2) of G1 are marked with purple or white arrows, respectively, based on Whi5-RFP localization. Images were deconvolved and summed. Bar, 5 µm. See also Supplemental Figure S1. (Ad) Percentage of unbudded cells with polarized Spa2 at 2 h after shifting to 37°C. Mean ± SEM is shown from analyses of cells in T_1 and T_2. Student's *t* tests were used, with the following notation: ns (not significant) for $p \geq 0.05$, ***$p < 0.001$, and ****$p < 0.0001$. (B) Normalized global intensity of Spa2-GFP in unbudded cells at 2 h after shifting to 37°C. Mean ± SEM is shown (see details in *Materials and Methods*).

emergence. In haploid cells, which bud in the axial pattern, Cdc42 is activated by Bud3 in early G1 prior to its activation by Cdc24 (Kang *et al.*, 2014). This stepwise Cdc42 activation occurs in correlation with the nuclear exit of the transcriptional repressor Whi5 (Kang *et al.*, 2014), which partitions G1 into two phases—T_1 and T_2 (Di Talia *et al.*, 2007). While biphasic activation of Cdc42 provides important insights into the temporal steps of bud-site assembly, the underlying mechanism has been less clear. Cells budding in a random pattern such as *rsr1*Δ exhibit occasional sporadic elevation of Cdc42-GTP during T_1. Yet robust Cdc42 polarization occurs similarly during T_2 in wild-type (WT) and mutant cells (Lee *et al.*, 2015). These observations raised critical questions: Is stepwise activation of Cdc42 necessary to ensure sequential execution of the processes leading to bud emergence in cells budding in any pattern? If so, is relatively less efficient Cdc42 polarization in *rsr1*Δ cells during the first phase sufficient for these cells to traverse the G1 phase? Is there an additional mechanism underlying Cdc42 polarization during the first phase of G1? Moreover, what are the sequential processes triggered by stepwise Cdc42 polarization? These questions led us to delve further into stepwise Cdc42 polarization. Here we report that biphasic Cdc42 polarization is coupled to stepwise assembly of a new septin ring. We also find that Rsr1 and Gic proteins have a partially redundant role in promoting Cdc42 polarization in the first phase of G1.

RESULTS AND DISCUSSION

cdc42 alleles that are defective at a distinct phase in G1

To investigate stepwise Cdc42 polarization further, we sought to identify *cdc42* alleles that exhibit polarization defects at either the first or second phase of G1. To this end, we examined temperature-sensitive (ts) *cdc42* mutants that arrest as unbudded cells at 37°C (Kozminski *et al.*, 2000) by time-lapse imaging of Spa2 fused to green fluorescent protein (GFP) as a marker for bud-site assembly, together with Whi5 fused to mCherry, a red fluorescent protein (RFP) to distinguish the first and second phases. Spa2 is one of the first proteins that localize to the incipient bud site prior to START, a cell-cycle commitment point in G1, and its localization is independent of Bem1 and Cdc24 (Snyder, 1989; Snyder *et al.*, 1991; Arkowitz and Lowe, 1997; Rida and Surana, 2005). Spa2 localized to the sites of polarized growth and to the bud neck during cytokinesis in WT cells after a shift to 37°C (Supplemental Figure S1a), consistent with previous reports. Spa2 localization was partially defective in the *cdc42-123* cells at 37°C mainly during the second phase (Figure 1A, b and d), and these cells became arrested with abnormal shapes (Supplemental Figure S1b). In contrast, Spa2 poorly polarized in *cdc42-118* cells at 37°C, and Whi5 often stayed longer in the nucleus (Supplemental Figure S1c). The *cdc42-118* cells that had already budded at temperature upshift maintained Spa2 polarization in the remaining cell cycle but failed to polarize and arrested as round, unbudded cells in the next G1 phase. A close examination of Spa2 polarization in unbudded cells with or without Whi5 in the nucleus revealed that Spa2 polarization is severely defective in *cdc42-118* cells from the first phase (Figure 1A, c and d), despite similar levels of Spa2 in unbudded cells after shifting to 37°C for 2–4 h (Figure 1B). These observations suggest that *cdc42-118* is unable to polarize in the first phase, which may lead to the sequential polarization defect in the second phase.

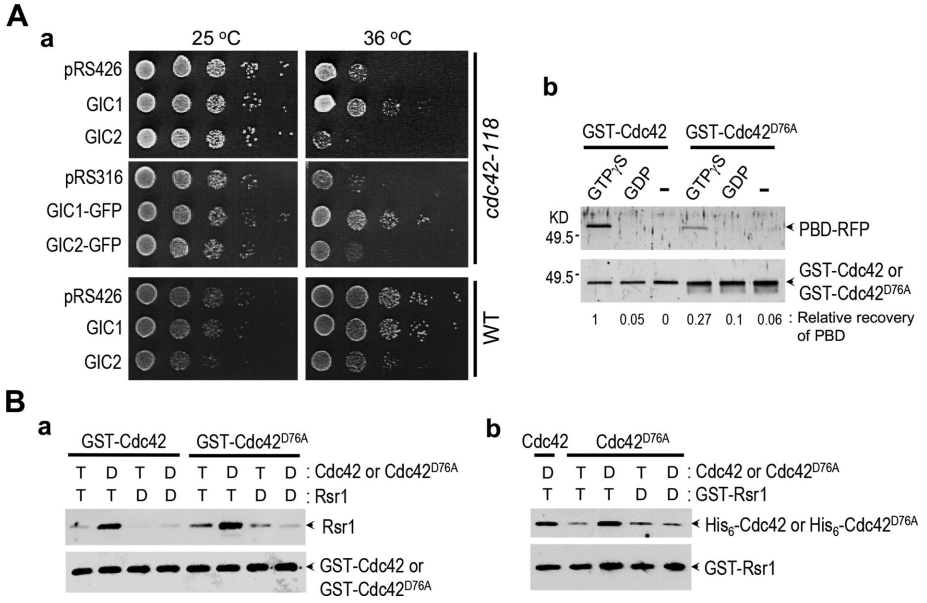

FIGURE 2: Cdc42^{D76A} poorly interacts with PBD. (Aa) Extra copies of *GIC1* suppress *cdc42-118*. A 10-fold serial dilution of each strain carrying an indicated plasmid was incubated at 25 or 36°C for 3 d on SC-Ura. (Ab) Cdc42^{D76A} poorly interacts with PBD-RFP. GST-Cdc42 or -Cdc42^{D76A}, preloaded with GTPγS or GDP or nucleotide-depleted (–), was incubated with yeast extract containing PBD-RFP at 4°C. Following GST pull-down assays, PBD-RFP and Cdc42 (or Cdc42^{D76A}) were detected with polyclonal antibodies against DsRed (top panel) and GST (bottom panel), respectively. Average relative recovery of PBD is shown below each lane. The WT control lanes have also been used for validation of the PBD-RFP biosensor (Okada *et al.*, 2017). (B) Cdc42^{D76A} interacts with Rsr1 equally well as WT Cdc42. Each purified GTPase, preloaded with GTPγS (T) or GDP (D), was incubated at 24°C in various combinations as indicated. (a) Following GST pull-down assays, Rsr1 and GST-Cdc42 (or -Cdc42^{D76A}) were detected with polyclonal antibodies against Rsr1 (top panel) and GST (bottom panel), respectively. (b) Following GST pull-down assays, His$_6$-Cdc42 (or Cdc42^{D76A}) and GST-Rsr1 were detected with polyclonal antibodies against Cdc42 (top panel) and GST (bottom panel), respectively.

Cdc42^{D76A} may be defective in its interaction with Gic proteins

To gain a deeper understanding of the first phase of Cdc42 polarization, we further characterized *cdc42-118*, which encodes Cdc42^{D76A} (Kozminski *et al.*, 2000). A previous genomewide study with *cdc42-118* identified synthetic-lethal or synthetic-sick interactions with *gic2*Δ and *rsr1*Δ (Kozminski *et al.*, 2003). Extra copies of *RSR1* suppress temperature-sensitive growth of *cdc42-118* and *gic1*Δ *gic2*Δ (Kozminski *et al.*, 2003; Gandhi *et al.*, 2006; Kang *et al.*, 2010), and *gic1*Δ *gic2*Δ is synthetic-lethal with *rsr1*Δ (Kawasaki *et al.*, 2003). Interestingly, we found that extra copies of *GIC1* from a low- or high-copy plasmid suppressed temperature-sensitive growth of *cdc42-118*, while extra copies of *GIC2* even made *WT* cells sick (Figure 2Aa). This web of genetic interactions suggested that the polarity establishment defect of *cdc42-118* and *gic1*Δ *gic2*Δ may result from a similar molecular deficiency.

Since Cdc42 directly interacts with Rsr1 (Kozminski *et al.*, 2003), we tested whether Cdc42^{D76A} is defective in interaction with Rsr1. After preloading Rsr1 and GST fusions of WT and the mutant Cdc42 with GTPγS (a nonhydrolysable GTP analogue) or GDP, these GTPases were incubated at 24°C in various combinations. The GST pull-down assays indicated that Rsr1-GTPγS preferentially associated with the GDP-loaded Cdc42 and Cdc42^{D76A} with similar efficiency (Figure 2Ba). In a complementary analysis, when GST-Rsr1 was pulled down, His$_6$-Cdc42 or Cdc42^{D76A} was recovered similarly (Figure 2Bb), suggesting that Cdc42^{D76A} is unlikely defective in interaction with Rsr1. We then tested whether Cdc42^{D76A} is defective in interaction with Gics using PBD-RFP, which contains the Gic2 PBD (Tong *et al.*, 2007). PBD interacted specifically with Cdc42-GTPγS, as expected, but poorly associated with Cdc42^{D76A}-GTPγS even at 4°C (Figure 2Ab). These data suggest that the poor interaction of Cdc42^{D76A} with Gics may account for its polarization defect in the first phase. Since other Cdc42 effectors also have a similar PBD, we next examined their interactions with Cdc42^{D76A} using yeast extracts carrying tagged Gic2, Cla4, or Ste20. Pull-down assays indicated that Gic2 was most defective in association with Cdc42^{D76A} (Supplemental Figure S2), consistent with the in vitro assay (Figure 2Ab), while Cla4 and Ste20 were also defective in association with Cdc42^{D76A} to different extents. Collectively, these data suggest that Cdc42^{D76A} is primarily, albeit not exclusively, defective in interaction with Gics.

Rsr1 and Gics may share a role in Cdc42 polarization during the first phase of G1

Consistent with a previous report (Kawasaki *et al.*, 2003), we observed that cells became arrested as large, unbudded cells when Rsr1 and both Gics were depleted (87%, $n = 470$), whereas cells depleted only for *GIC1* and *GIC2* continued budding (Supplemental Figure S3A). Why do the cells lacking Rsr1 and Gics fail to bud despite the presence of all components implicated in symmetry breaking? On the basis of the genetic interactions among *cdc42-118*, *rsr1*Δ, and *gic1*Δ *gic2*Δ and the compromised interaction between Cdc42^{D76A} and Gic proteins (see above), we postulated that cells lacking Rsr1 and both Gics might be defective in the first phase of Cdc42 polarization. To test this idea, we examined Cdc42 polarization in the P_{GAL}-*GIC1 gic2*Δ *rsr1*Δ strain expressing PBD^{W23A}-tdTomato (PBD-RFP), an improved Cdc42-GTP probe (Okada *et al.*, 2013), by time-lapse imaging. When *GIC1* was expressed, Cdc42 polarized normally: a strong Cdc42-GTP cluster developed in mother cells within 30 min after the onset of cytokinesis (68%, $n = 25$; Figure 3Aa), while PBD-RFP fluctuated for a longer time in daughter cells until a strong Cdc42-GTP cluster developed. However, when *GIC1* expression was turned off, only a few mother cells exhibited new development of PBD-RFP signal within 1–2 h after cytokinesis (10%, $n = 40$; Figure 3Ab); instead, the PBD signal was evident as puncta on the cell periphery, as also shown in the kymograph of PBD-RFP along the cell cortex (Figure 3, Ab and Bb). Quantitative analyses of the PBD clusters in mother cells indicated that strong Cdc42 polarization occurred soon after the onset of cytokinesis when *GIC1* was expressed (Figure 3C; Gal) but not when *GIC1* expression was turned off (Glu). Since global intensity of GFP-Cdc42 in the P_{GAL}-*GIC1 gic2*Δ *rsr1*Δ cells slightly increased after shifting cells to the glucose-based medium (Supplemental Figure S3Ac), the defect of Cdc42 polarization is not due to reduced protein level. Interestingly, when *GIC1* was overexpressed under the *GAL* promoter, the Cdc42-GTP cluster level was highly elevated before the axis of Cdc42 polarization became stabilized, which occurs around the

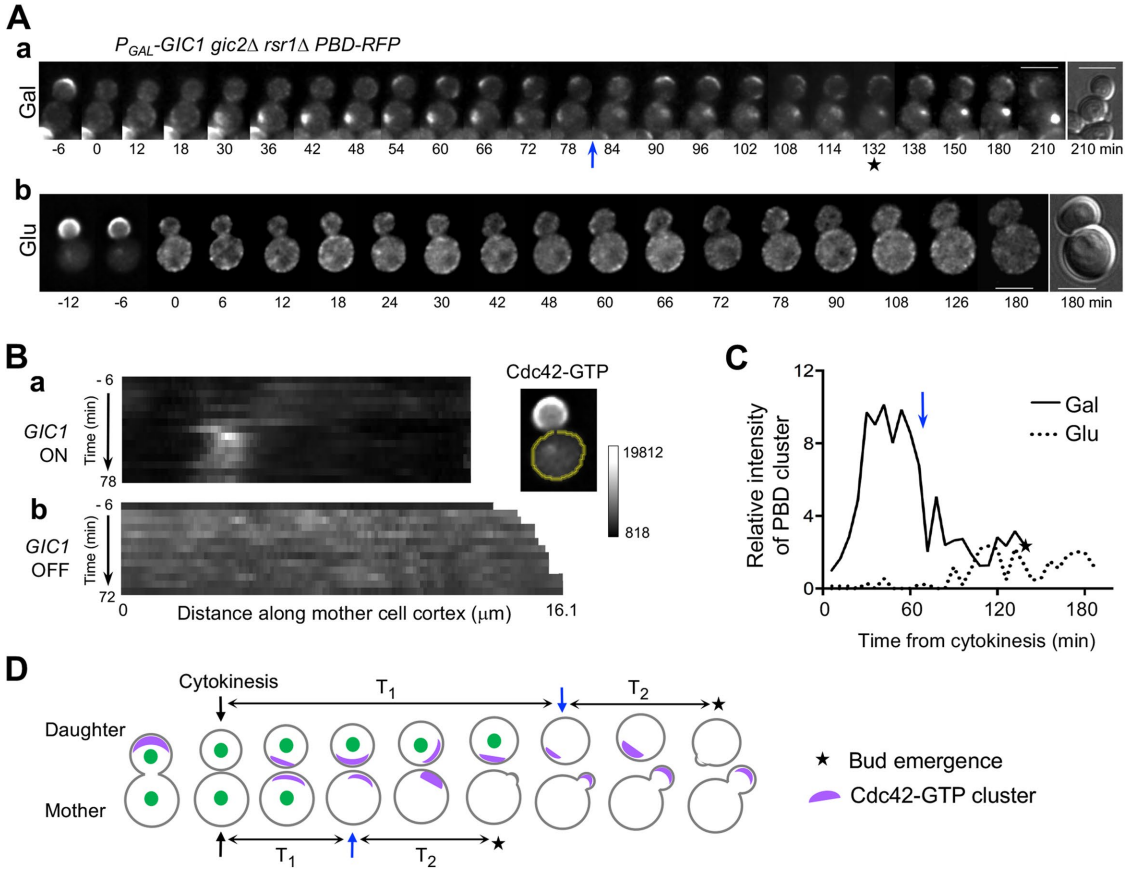

FIGURE 3: Cells lacking Gics and Rsr1 are defective in the first step of Cdc42 polarization. (A) Cdc42 polarization (a) with or (b) without *GIC1* expression in the P_{GAL}-*GIC1 gic2Δ rsr1Δ* PBD^{W23A}-*RFP* cells. Numbers denote approximate time (min) relative to the onset of cytokinesis (estimated from the PBD intensity). Bars, 5 μm. (B) Kymograph of PBD fluorescence along the cell cortex (e.g., a yellow line of an image) from 6 min prior to the estimated onset of cytokinesis until approximate T_1–T_2 transition (when *GIC1* was on) or for a comparable time window (when *GIC1* was off). (C) A representative analysis of PBD cluster in mother cells with (Gal) or without (Glu) *GIC1* expression. The intensity of PBD cluster at each time point is shown as a relative ratio to its intensity at the estimated onset of cytokinesis ($t = 0$). (D) Scheme of Cdc42 polarization (shown in purple) in two steps during T_1 and T_2, partitioned by the nuclear exit of Whi5 (green). Blue arrows in Aa, C, and D mark the approximate T_1–T_2 transition after which Cdc42 polarization site becomes stabilized, and stars mark when cells undergo bud emergence (also in the mother cell in Aa and C).

beginning of T_2 (see blue arrows in Figure 3; see Figure 3D), while its peak level during the second phase was elevated ~3~4-fold relative to its intensity at the onset of cytokinesis (Figure 3C; Lee *et al.*, 2015). Collectively, these results suggest that Rsr1 and Gics share a role in Cdc42 polarization in the first phase of G1.

The role of Rsr1 in Cdc42 polarization depends on spatial cues

If the role of Rsr1 in Cdc42 polarization is dependent on spatial cues, as in the case of bud-site selection, we would expect that *gic1Δ gic2Δ* would be lethal in the absence of spatial cues (even with WT *RSR1*). To test this idea, we analyzed meiotic progeny of a diploid generated by crossing *gic1Δ gic2Δ* with *axl2Δ rax1Δ*. Deletion of *AXL2* and *RAX1* is expected to remove both functional axial and bipolar landmarks (Roemer *et al.*, 1996; Kang *et al.*, 2004). We found 6 of 88 meiotic progenies that were expected unambiguously to harbor the *axl2Δ rax1Δ gic1Δ gic2Δ* quadruple mutation did not germinate after 2.5 d at 30°C, although four spores germinated and formed microcolonies after 4 d (Supplemental Figure S3B). Because of the possible occurrence of spontaneous suppressor mutations and because of the presence of some dead segregants (whose genotype could not be determined), the lethality of the *axl2Δ rax1Δ gic1Δ gic2Δ* mutant may be higher. Since there were some ambiguities in this genetic analysis, we performed an additional test by generating a P_{GAL}-*GIC1 gic2Δ axl2Δ rax1Δ* strain. When this strain was imaged after turning off *GIC1* expression, the majority of these cells arrested as large unbudded cells during a 5–6 h period (89%, $n = 200$; Supplemental Figure S3C). The 11% of cells that had undergone bud emergence did so within 1 h after turning off *GIC1* expression, and this is likely due to some remaining Gic1 in these cells, as Gic1 is a relatively stable protein (Höfken and Schiebel, 2004). Therefore, we conclude that the role of Rsr1 in Cdc42 polarization in the first phase depends on spatial cues.

Biphasic Cdc42 polarization may be coupled to stepwise assembly of the septin ring

Why does Cdc42 polarization occur in two steps during G1? Since Cdc42 and Gics are necessary for septin organization (Gladfelter *et al.*, 2002; Iwase *et al.*, 2006; Okada *et al.*, 2013), we tested whether

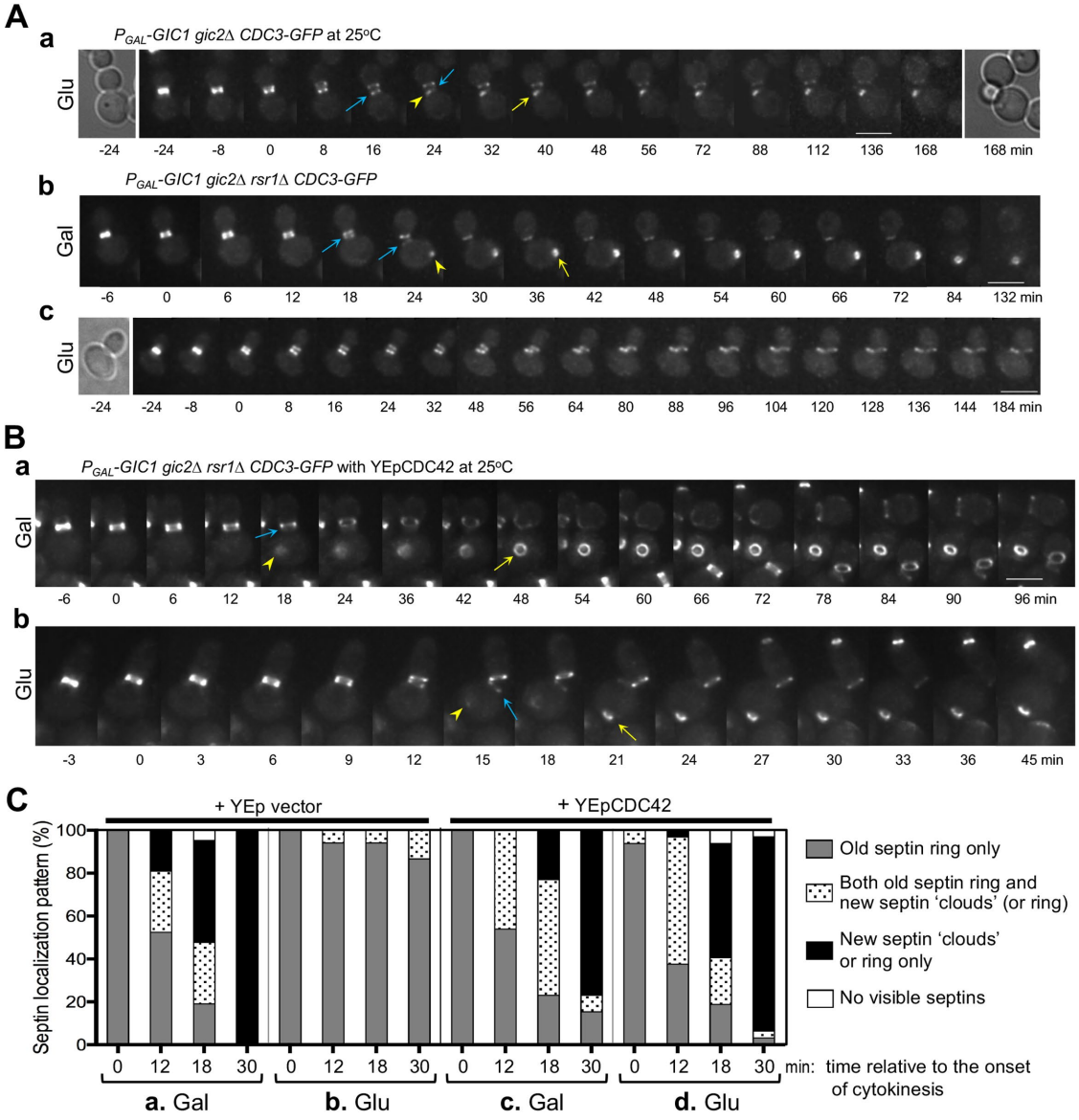

FIGURE 4: Cells lacking Gics and Rsr1 are defective in septin recruitment, and this defect is rescued by extra copies of *CDC42*. (Aa) Localization of Cdc3-GFP in the P_{GAL}-*GIC1 gic2*Δ *CDC3-GFP* cells after turning off *GIC1*. (Ab,Ac) Localization of Cdc3-GFP in the P_{GAL}-*GIC1 gic2*Δ *rsr1*Δ *CDC3-GFP* cells before (b) or after (c) turning off *GIC1* expression. Numbers denote time (min) relative to the onset of cytokinesis (when the septin ring splits into a double ring). Blue and yellow arrows mark old and new septin rings, respectively; arrowheads mark new septin "clouds." Bars, 5 µm. (B) Localization of Cdc3-GFP in the same strain used in Ab and Ac, except carrying YEpCDC42 before (a) or after (b) turning off *GIC1* expression. See legend to A. (C) Summary of septin localization patterns in the P_{GAL}-*GIC1 gic2*Δ *rsr1*Δ *CDC3-GFP* cells carrying YEp empty vector (a, b) or YEpCDC42 (c, d) and before (a, c) or after (b, d) turning off *GIC1* expression. Analyses at the selected time points from the following number of time-lapse images are plotted: $n = 21$ (a), 15 (b), 13 (c), and 32 (d).

cells lacking Gics and Rsr1 are defective in either recruitment of the septins (appearing as disorganized "clouds") or ring formation by time-lapse imaging of Cdc3-GFP. Even when both Gics were depleted, new septin clouds often appeared prior to disassembly of the old ring in the presence of *RSR1* (98%, $n = 16$; Figure 4Aa). In contrast, in the absence of Rsr1 and Gic2, new septin clouds appeared soon after cytokinesis only when *GIC1* was expressed (100%, $n = 12$; Figure 4Ab). When *GIC1* expression was turned off, the majority of P_{GAL}-*GIC1 gic2*Δ *rsr1*Δ cells failed to form new septin clouds or ring after cytokinesis (90%, $n = 20$; Figure 4Ac); instead, the old septin ring remained in these cells long after cytokinesis, and cells arrested in the unbudded state. In a few cells, new Cdc3-GFP signal appeared after cytokinesis, but the signal was weak and transient without developing into a septin ring. Taken together, these results suggest that Rsr1 and Gics share a role in recruitment of new septins in the first phase of Cdc42 polarization. These observations are consistent with the idea that biphasic Cdc42 polarization is coupled to stepwise assembly of the septin ring—first, septin recruitment, and then ring assembly (Iwase *et al.*, 2006)—and is thus unlikely limited to cells budding in the axial pattern.

Overexpression of Cdc42 bypasses requirement of Rsr1 and Gics for septin recruitment

As discussed above, Cdc42 polarization in the first phase and septin recruitment require either Rsr1 or Gics. Although Gics could function in septin recruitment as downstream effectors of Cdc42, we considered another possibility that Gics might share a role with Rsr1 in promoting Cdc42 polarization. If this is the case, then an elevation of Cdc42 might be able to bypass the requirement of Rsr1 and both Gics in septin recruitment. To test this idea, we examined the localization of septin in the P_{GAL}-*GIC1 gic2*Δ *rsr1*Δ cells carrying a multicopy CDC42 plasmid. Remarkably, these cells were able to recruit new septins even when Rsr1 and both Gics were absent (Figure 4Bb). We compared septin localization patterns at selective time points from time-lapse images. The cells carrying the CDC42 plasmid had either new septin "clouds" or ring within 30 min after cytokinesis even when Rsr1 and both Gics were depleted, unlike cells with a vector control (compare d to b, Figure 4C). This timing of new septin assembly in cells overexpressing Cdc42 was comparable to cells expressing *GIC1* (Figure 4, Ba, Ca, and Cc). These results are consistent with the idea that extra copies of Cdc42 allow its polarization and thus trigger septin recruitment in the absence of Gics and Rsr1. Together with the data discussed above, these findings support the idea that Gics and Rsr1 share a role in promoting Cdc42 polarization during T_1, which leads to septin recruitment.

Gics may promote Cdc42 polarization by stabilizing Cdc42 on the plasma membrane

How do Gic proteins promote Cdc42 polarization? Although Gics bind to Cdc42-GTP, Gic1 has additional membrane association domains and polarizes even when Cdc42 binding is disrupted (Chen *et al.*, 1997; Takahashi and Pryciak, 2007). We hypothesized that Gics might promote Cdc42 polarization by slowing its mobility on the plasma membrane (PM). To test this idea, we compared Cdc42 dynamics in WT and *gic1*Δ *gic2*Δ cells by fluorescence recovery after photobleaching (FRAP) analysis. Indeed, we found that Cdc42 cluster at the incipient bud site recovered faster after bleaching in *gic1*Δ *gic2*Δ cells than in WT (Figure 5A). This role of Gics may be more critical at a higher temperature, since haploid *gic1*Δ *gic2*Δ cells often fail to establish cell polarity at 37°C (or at 32°C in some strain backgrounds) (Brown *et al.*, 1997; Chen *et al.*, 1997; Bi *et al.*, 2000). It is possible that Cdc42 is more dynamic on the PM at a higher temperature, and thus its polarization is more dependent on Gics even when Rsr1 is present. Consistent with the idea, Cdc42 was more mobile at the incipient bud site at 34°C (a semipermissive temperature for the *gic1*Δ *gic2*Δ strain used in this study) than at 22°C (Figure 5Ab).

There has been considerable debate about whether Cdc42 polarizes independently of guanine nucleotide dissociation inhibitors (GDIs) and actin-based trafficking (Marco *et al.*, 2007; Slaughter *et al.*, 2009; Layton *et al.*, 2011; Freisinger *et al.*, 2013; Jose *et al.*, 2013; Klunder *et al.*, 2013; Slaughter *et al.*, 2013; Bendezu *et al.*, 2015; Woods *et al.*, 2016). Interestingly, both fission and budding yeast cells expressing a *cdc42* mutation (*cdc42-ritC*), in which the CAAX sequence is replaced by the C-terminal amphipathic helix of a Rit GTPase, are able to undergo symmetry breaking, suggesting that Cdc42 can polarize independently of both GDI-mediated membrane extraction of Cdc42-GDP and vesicle trafficking (Bendezu *et al.*, 2015). Since the budding yeast *cdc42-ritC* mutant is temperature sensitive and exhibits frequent loss of singularity of budding, we speculated that slower mobility of Cdc42-ritC might allow its polarization but result in poor competition between Cdc42 clusters. Indeed, we found that Cdc42-ritC-GFP exhibited much slower recovery than WT Cdc42 after bleaching (Figure 5B).

Since Cdc42-ritC exhibits slower dynamics than WT Cdc42, we wondered whether the *cdc42-ritC* mutant can bypass requirement of Rsr1 or Gics for its polarization during the first phase of G1. Surprisingly, however, when we tested genetic interactions between *cdc42-ritC gic1*Δ and *gic2*Δ, we found all meiotic progeny that could be predicted unambiguously to harbor all *cdc42-ritC, gic1*Δ, and *gic2*Δ mutations were inviable (Figure 5Ca). In contrast, a similar genetic test with *rsr1*Δ indicated that all meiotic progeny (except one) from 88 tetrads, including the triple *cdc42-ritC gic1*Δ *rsr1*Δ mutant, were viable (Figure 5Cb). Therefore, polarization of Cdc42-ritC is likely to be mediated by Gics during the first phase of G1. This observation seems counterintuitive because Cdc42-ritC is less mobile than WT Cdc42, which is more mobile in the *gic1*Δ *gic2*Δ cells (see Figure 5Ab). A possible explanation for the synthetic lethality of *cdc42-ritC gic1*Δ *gic2*Δ is that even a slight increase of its mobility (in the absence of Gic1/2) could be more detrimental to polarization of Cdc42-ritC, which presumably occurs via lateral diffusion and/or GDI-independent exchanges between membrane and cytosol. The *cdc42-ritC* mutant is also defective in bud-site selection (Bendezu *et al.*, 2015), consistent with our conclusion that its polarization is mediated via Gics, rather than Rsr1, and thus *cdc42-ritC* is likely inviable in the absence of Gics. Collectively, these results suggest that Gics promote Cdc42 polarization by stabilizing Cdc42 on the PM.

Model for biphasic Cdc42 polarization in G1

In this study, we show that Rsr1 and Gic1/Gic2 share a common role in Cdc42 polarization during the first phase of G1 and that Cdc42 polarization in the first phase is necessary for septin recruitment. We thus suggest that biphasic Cdc42 polarization is coupled to stepwise assembly of the new septin ring and is involved in both spatial cue-dependent and spontaneous cell polarization (Figure 5D). But how Cdc42 polarization promotes septin recruitment remains an open question. Gic proteins are known to be involved in septin assembly by directly interacting with septin subunits and stabilizing the septin complex (Iwase *et al.*, 2006; Sadian *et al.*, 2013). Since overexpression of *CDC42* can bypass the requirement of Gic1/2 and Rsr1 for septin recruitment (Figure 4), Cdc42 is able to promote septin recruitment without Gics. An interesting possibility is that Cdc42 may recruit septins directly or via other proteins such as Axl2, as previously suggested (Gao *et al.*, 2007).

While Gic proteins interact with Cdc42-GTP, involvement of Gics in Cdc42 polarization suggests a previously unrecognized positive feedback loop (Figure 5D). Initial stochastic activation of Cdc42 may recruit Gics by interacting with their PBD. The Gic-Cdc42-GTP complex may be stabilized through the interaction with PIP_2 on the PM (Takahashi and Pryciak, 2007; Orlando *et al.*, 2008). This stabilization may counteract lateral diffusion of Cdc42, the endocytosis-mediated internalization, and/or GDI-mediated recycling (Ozbudak *et al.*, 2005; Marco *et al.*, 2007; Slaughter *et al.*, 2009; Klunder *et al.*, 2013; Woods *et al.*, 2016), consistent with our FRAP data (Figure 5A).

Cdc42 polarization mediated by Rsr1 may involve a positive feedback loop, which includes spatial cue-dependent recruitment and/or activation of the Rsr1 GTPase module and local activation of Cdc42 (Kozminski *et al.*, 2003; Kang *et al.*, 2014; Lee *et al.*, 2015). Rsr1 may also be involved in the second phase of Cdc42 polarization via interaction between Rsr1-GTP and Cdc24

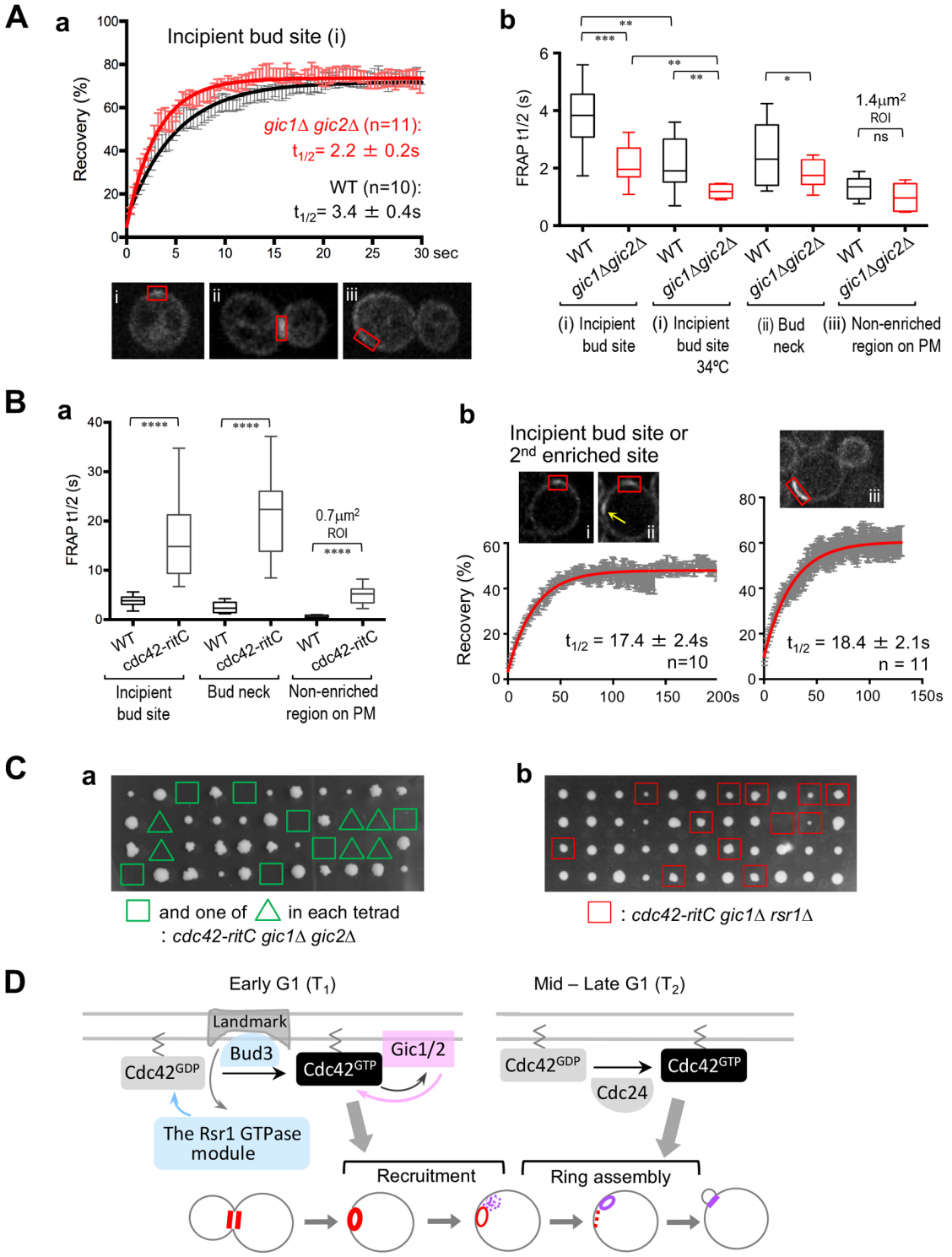

FIGURE 5: Gic proteins may promote Cdc42 polarization by stabilizing Cdc42 on the PM. (Aa) FRAP analyses of GFP-Cdc42 at the incipient bud site in WT and *gic1*Δ *gic2*Δ cells (mean ± SEM shown). (Ab) Halftimes of GFP-Cdc42 FRAP recovery at indicated sites; all at 22°C, except those indicated at 34°C. For each data point, $n = 9–11$. Student's *t* tests were used, with the following notation: ns (not significant) for $p \geq 0.05$, *$p < 0.05$, **$p < 0.01$, ***$p < 0.001$, and ****$p < 0.0001$. (Ba) Halftimes of FRAP recovery of GFP-Cdc42-ritC vs. GFP-Cdc42 at each site. $n = 9–11$ for each data point. (Bb) FRAP curves of GFP-Cdc42-ritC at each indicated site. See legend to Aa and Ab. (C) Representative tetrads from crosses between *cdc42-ritC gic1*Δ and *gic2*Δ (a) and between *cdc42-ritC gic1*Δ and *cdc42-ritC rsr1*Δ (b). Segregants marked with green squares and one of each pair marked with green triangles harbor the *cdc42-ritC gic1*Δ *gic2*Δ mutation. Segregants marked with red squares harbor the *cdc42-ritC gic1*Δ *rsr1*Δ mutation. (D) Model for biphasic Cdc42 polarization coupled to stepwise assembly of a new septin ring. Red and purple rings denote old and new septin rings, respectively. Purple dots and dotted red line denote newly recruited septin "clouds" and disassembling old ring, respectively (see the text).

(Zheng *et al.*, 1995; Park *et al.*, 1997). We anticipate that the first phase of Cdc42 polarization and the initial recruitment of septins do not require Cdc24, because Cdc42 is activated by Bud3 in the first phase (Kang *et al.*, 2014), during which Cdc24 is mostly sequestered within the nucleus in haploid cells (Toenjes *et al.*, 1999; Nern and Arkowitz, 2000; Shimada *et al.*, 2000). The second step of Cdc42 polarization and thus septin ring assembly are likely promoted by Cdc24 and Bem1. Consistent with this timing, Cdc24 activity is stimulated by Bem1 (Smith *et al.*, 2013; Rapali *et al.*, 2017), which associates with Cdc24 after START (Witte *et al.*, 2017). While further investigation is necessary to fully understand the underlying mechanisms, biphasic Cdc42 polarization provides an elegant example of a highly redundant system, which integrates distinct signals to achieve a single biological event.

MATERIALS AND METHODS

Strains, plasmids, and growth conditions

Standard methods of yeast genetics, DNA manipulation, and growth conditions were used (Guthrie and Fink, 1991). All yeast strains used for imaging express tagged proteins under their native promoters from the chromosomes. Yeast strains were grown in rich yeast medium YPD (yeast extract, peptone, dextrose) or synthetic complete (SC) containing 2% dextrose as a carbon source, unless stated otherwise. Where indicated, SC medium containing 2% galactose (SGal) was used instead of dextrose to turn on the *GAL* promoter. To track the segregation of auxotrophic markers and to maintain plasmids, strains were cultured in SC medium lacking the appropriate nutrient(s) (e.g., SC-Ura). Strains used in this study are listed in Supplemental Table S1. Multicopy plasmids pRS426-GIC1 and pRS426-GIC2 (2μ, URA3) were kind gifts from R. Tabtiang and I. Herskowitz (University of California, San Francisco). Low-copy plasmids pRS316-GIC1-GFPx3 and pRS316-GIC2-GFPx3 (CEN, URA3) were kind gifts from P. Pryciak (University of Massachusetts Medical School) (Takahashi and Pryciak, 2007). Plasmids used for expression of GST-Cdc42 and His_6-Cdc42 and a multicopy plasmid YEp103-CDC42 were previously described (Kozminski *et al.*, 2003). Plasmids for expression of GST-$Cdc42^{D76A}$ and His_6-$Cdc42^{D76A}$ were generated by subcloning using pKK655 carrying the *cdc42-118* allele and each corresponding WT CDC42 plasmid. The D76A mutation was confirmed by digestion with *Pst*I, as previously described (Kozminski *et al.*, 2000). The plasmid used for expression of GST-Rsr1 was previously described (Holden *et al.*, 1991). The plasmids used for expression of movable open reading frame (MORF)-tagged Gic2, Ste20, and Cla4 were previously described (Gelperin *et al.*, 2005) and purchased from Thermo Scientific Open Biosystems.

Microscopy and image analysis

Cells were grown in an appropriate synthetic medium overnight and then freshly subcultured for 3–4 h in the same medium. For most time-lapse imaging, images were captured (11 or 13 z-stacks; 0.3 μm step) every 3 or 6 min with cells either mounted on a 2% agarose slab or a glass-bottomed dish (MatTek) containing the indicated medium with 5 μM propyl gallate (Sigma), an anti-fade reagent, as previously described (Kang *et al.*, 2014; Miller *et al.*, 2017). The slab or dish was put directly on a stage (at 25–26°C) or in a temperature-control chamber set to either 30 or 37°C, as indicated. All time-lapse imaging at 37°C started at 30 min after temperature upshift. For imaging the P_{GAL}-*GIC1* strains after turning off *GIC1* expression, cells grown in galactose-based medium were washed with glucose-based medium twice prior to seeding on a glass-bottomed dish, and time-lapse imaging was then started ~30 min after a shift to glucose-based medium at 25°C. Fluorescence microscopic images in all figures, except Figure 5, were captured using a Nikon Ti-E microscope fitted with a 100×/1.45 NA Plan-Apochromat Lambda oil immersion objective lens (Nikon), FITC (fluorescein isothiocyanate)/GFP and mCherry/TexasRed filters from Chroma Technology, an Andor iXon Ultra 888 electron-multiplying charge-coupled device (EM CCD) (Andor Technology), and the software Nis elements (Nikon). DIC (differential interference contrast) images in Supplemental Figure S3 were captured (13 z-stacks; 0.4-μm step) every 10 or 20 min at 24–25°C using a Nikon E800 microscope fitted with a 100×/1.30 NA oil-immersion objective lens, Hamamatsu ORCA-2 CCD (Hamamatsu Photonics), and Slidebook software (Intelligent Imaging Innovations), and single z-stack images were used to make figures.

To image Spa2-GFP and Whi5-RFP in WT and *cdc42* mutants, cells grown at 24–25°C overnight were mounted on glass-bottomed dishes and initially imaged at 25°C for 1 h to ensure healthy growth. Two-color time-lapse imaging was then started at 30 min after temperature upshift to 37°C. Image processing and analyses were performed using ImageJ (National Institutes of Health). Where indicated, images were deconvolved by the Iterative Constrained Richard-Lucy algorithm using Nis element software. Summed intensity projections of z-stacks of representative time-lapse images were used to generate Figure 1 and Supplemental Figure S1. Images at 2 h after shifting to 37°C were analyzed to compare Spa2-GFP polarization in unbudded cells during T_1 (from cytokinesis until mid G1 when Whi5-RFP resides in the nucleus) and T_2 (from mid-G1 when Whi5-RFP intensity in the nucleus drops less than 50% until bud emergence or G1 arrest for mutants) (Figure 1). A fluorescence threshold was set to select polarized Spa2-GFP and measure the mean intensity of polarized Spa2-GFP using the summed WT images of z-stacks after background subtraction. The same threshold was also applied to all mutant images that were captured and processed using the same conditions. Unbudded cells (in T_1 or T_2) that had polarized Spa2-GFP were counted from three to five sets of time-lapse images of each strain, and mean ± SEM is shown by analyzing the following total number of cells at each phase: WT, $n = 111$ (T_1) and 71 (T_2), *cdc42-123*, $n = 129$ (T_1) and 70 (T_2), and *cdc42-118*, $n = 245$ (T_1) and 87 (T_2). To compare total Spa2-GFP level in individual cells of each strain after temperature upshift, global intensity of Spa2-GFP in unbudded cells was quantified using the same summed intensity projections (at 2–4 h after temperature upshift to 37°C). A region of interest (ROI) was drawn around the outline of unbudded cells, and integrated density of each ROI was measured in three sets of time-lapse images for each strain, counting a total number of cells: $n = 80$ (WT), 110 (*cdc42-123*), and 100 (*cdc42-118*) (Figure 1B). For quantification of global intensity of GFP-Cdc42 (Supplemental Figure S3Ac), average intensity projections were created from all 15 z-sections at 0.3-μm spacing, and an ROI was drawn around the outline of unbudded cells. WT cells without any fluorescently tagged protein were mixed to capture control cell images together with experimental strains, and the mean intensity of the control cells was used to subtract background.

The PBD fluorescence intensity along the cell cortex was analyzed using single focused z-stack images of HPY2618 (P_{GAL}-*GIC1 gic2*Δ *rsr1*Δ PBD^{W23A}-*tdTomato*) when *GIC1* was expressed (Gal) from 6 min prior to the onset of cytokinesis (estimated based on PBD distribution) until T_1–T_2 boundary (estimated based on stabilization of the PBD cluster location) (Okada *et al.*, 2013; Lee *et al.*, 2015) (see Figure 3D). We noticed that the PBD-RFP probe was slightly toxic in this strain background, making cells grow slowly, particularly in galactose-based medium. Images of cells when *GIC1* was turned off (Glu) were also analyzed from 6 min prior to cytokinesis and subsequent time points (although the exact cell-cycle stage

of the end point was not clear due to lack of single PBD cluster development when *GIC1* was not expressed). To quantify PBD fluorescence intensity around the cell cortex using ImageJ, freehand lines were drawn by selecting a three-pixel (0.389 µm)-wide region around the cell periphery, and PBD-RFP fluorescence was then measured along the lines for each time point of time-lapse images. Kymographs were generated by displaying PBD intensity in the same scale for both cases when *GIC1* was on or off (Figure 3B). Maximum intensity projections of z-stacks were used to make figures of fluorescence images in Figures 3 and 4, except in Figure 3Ab, single z-stack images were used to show PBD fluorescence at the cell periphery more clearly.

To quantify Cdc42 polarization, the fluorescence intensity of PBD-RFP clusters was measured by a threshold method using an ImageJ macro (Okada *et al.*, 2013; Okada *et al.*, 2017). Briefly, mean projections were generated from five best z-sections at each time point, and then a threshold method was used after background subtraction. Mother and daughter cells of HPY2618 were analyzed separately from the onset of cytokinesis until bud emergence when cells were grown in galactose-based medium at 25°C and after shifting to glucose-based medium from the onset of cytokinesis over 4 h at the same temperature. The intensity of PBD-RFP clusters at each time point were normalized to its value at the onset of cytokinesis ($t = 0$). A representative analysis of PBD-RFP cluster in a mother cell of the P_{GAL}-*GIC1 gic2*Δ *rsr1*Δ *PBD*^{W23A}-*tdTomato* strain is shown when *GIC1* was expressed (Gal) and when *GIC1* expression was turned off (Glu) (Figure 3C). These cells rarely underwent new budding when *GIC1* expression was turned off.

FRAP analysis

Cells were grown in an appropriate synthetic medium overnight and then freshly subcultured for 3–4 h in the same medium. FRAP experiments (and images shown in Figure 5) were performed at 22°C, except those indicated at 34°C, using a spinning disk confocal microscope (Ultra-VIEW VoX CSU-X1 system; Perkin Elmer-Cetus) equipped with a 100×/1.4 NA Plan Apochromat objective lens (Nikon); 440-, 488-, 515-, and 561-nm solid-state lasers (Modular Laser System 2.0; Perkin Elmer-Cetus), and a back-thinned EM CCD (ImagEM C9100-13; Hamamatsu Photonics) on an inverted microscope (Ti-E; Nikon). Images were captured at a single z-section on a gelatin slab using the photokinesis unit on the Ultra-VIEW VoX confocal system, similarly to the assays described previously (Coffman *et al.*, 2009; Miller *et al.*, 2017). After collecting five prebleach images, selected ROI's were bleached to <55% of the original fluorescence intensity. Postbleach images were captured for a duration long enough so the fluorescence recovery curve reached a plateau. For each FRAP experiment, all intensity values (after correcting for background and photobleaching) were normalized, so the prebleaching and the first postbleaching intensities equal 100 and 0%, respectively. To reduce noise, the intensities of every three consecutive postbleach time points were averaged. Then the intensity data from individual ROIs and the average intensity value at each time point across all ROIs were plotted and fitted using the exponential decay equation $y = m_1 + m_2 \exp(-m_3 x)$, where m_3 is the off-rate, using Prism 6 (GraphPad Software). The halftime of recovery was calculated using the equation $t_{1/2} = \ln 2/m_3$.

Halftimes of GFP-Cdc42 FRAP recovery in WT and *gic1*Δ *gic2*Δ cells were compared at the following sites: the incipient bud site of unbudded cells ($n = 10$, WT; $n = 11$, *gic1*Δ *gic2*Δ), bud neck ($n = 11$, WT; $n = 11$, *gic1*Δ *gic2*Δ), and nonenriched region on the PM of large budded cells ($n = 10$, WT; $n = 11$, *gic1*Δ *gic2*Δ) at 22°C and also at the incipient bud site of unbudded cells at 34°C ($n = 10$, WT; $n = 9$, *gic1*Δ *gic2*Δ). Halftimes of GFP-Cdc42-ritC FRAP recovery were also determined at the incipient bud site ($n = 10$), bud neck ($n = 9$), and nonenriched region on the PM of large budded cells ($n = 8$) and compared with those of GFP-Cdc42 at 22°C. Either a FRAP curve (with mean ± SEM) or a bar graph (with median, quartiles, maximum, and minimum) are plotted using Prism 6.

Protein purification, in vitro binding assay, and immunoblotting

GST-Rsr1, His_6-Cdc42, and His_6-Cdc42^{D76A} were expressed and purified in a protease-deficient *Escherichia coli* strain (BL21 codon plus), and GST-Cdc42 and GST-Cdc42^{D76A} were expressed from insect cell lines, as previously described (Kozminski *et al.*, 2003). Either purified proteins or high-speed supernatants (2.5 µg total protein per reaction) of the insect cell extracts containing GST-Cdc42 or GST-Cdc42^{D76A} were used in binding assays, as previously described (Kozminski *et al.*, 2003). Briefly, purified GTPases (either with or without GST moiety) were dialyzed overnight at 4°C against a buffer (20 mM Tris-HCl, pH 7.5, 1 mM dithiothreitol [DTT], 5 mM $MgCl_2$, 10% glycerol) containing 2.5 µM GDP after purification. Approximately 1 µg of a GST-fusion protein was diluted to a final volume of 50 µl with 50% glutathione Sepharose bead slurry and incubated for 1 h at 4°C. The beads were collected by centrifugation and resuspended in Buffer I (20 mM Tris-HCl, pH 7.5, 100 mM NaCl, 1 mM DTT, 10 mM EDTA, 10% glycerol, 0.1% Triton X-100, 10 µg/ml leupeptin, 10 µg/ml aprotinin). After incubation for 1 h at room temperature, Buffer I was substituted with Buffer I containing 5 mM $MgCl_2$ plus 0.5 mM GTPγS or 0.5 mM GDP (Roche Diagnostics). After 30 min incubation at 24°C, the beads were resuspended in Buffer I containing 10 mM $MgCl_2$ plus 0.5 mM GTPγS or 0.5 mM GDP instead of 10 mM EDTA and then incubated 20 min at 24°C to stabilize the nucleotide bound state of the GTPase. For in vitro binding reaction, Rsr1 (~400 nM), purified after removal of GST, was preloaded with GTPγS or GDP and incubated with GST-Cdc42 or GST-Cdc42^{D76A} (~400 nM each), which was also preloaded with GTPγS or GDP in various combinations at 24°C. Association of Cdc42 or Cdc42^{D76A} with GST-Rsr1 was determined similarly, except GST-Rsr1, His_6-Cdc42, and His_6-Cdc42^{D76A} were used in various combinations, as indicated. The interaction between PBD-RFP and GST-Cdc42 (or GST-Cdc42^{D76A}) was tested by similar binding assays, except that the soluble fraction (S10) of extracts from 80 OD_{600} units of yeast cells (HPY1231), which express Gic2-PBD-RFP from the chromosome, was used, and the incubation was performed at 4°C. GST-Cdc42, GST-Cdc42^{D76A}, and GST-Rsr1 were detected by immunoblotting with polyclonal antibodies against GST (Santa Cruz Biotechnology). Rsr1 (after GST was removed), His_6-Cdc42, and Gic2-PBD-RFP were detected with polyclonal antibodies against Rsr1 (Park *et al.*, 1997), Cdc42 (Kozminski *et al.*, 2003), and DsRED (Clontech Laboratories), respectively. In vitro binding assays were repeated three times from two independent preparations of purified proteins or yeast extracts.

To test the association of Cdc42 effectors with GST-Cdc42 or GST-Cdc42^{D76A}, Gic2, Cla4, or Ste20 was expressed as a triple affinity tagged (composed of His_6-HA epitope-immunoglobulin G (IgG) binding ZZ domain) protein in a yeast strain (Y258) using each MORF plasmid (Gelperin *et al.*, 2005). The pull-down assays of the MORF-tagged proteins were performed with IgG-Sepharose, as previously described (Gelperin *et al.*, 2005). GST fusion proteins were detected as described above, and each MORF-tagged protein was detected with monoclonal anti-HA antibodies (Covance, Emeryville, CA).

Statistical analysis

Data analysis was performed using Prism 6 (GraphPad Software). Error bars indicate SEM unless indicated otherwise. The bar graphs of FRAP data show median as a line, quartiles, maximum, and minimum. A two-tailed Student's *t* test was performed to determine statistical differences between two sets of data: ns (not significant) for $p \geq 0.05$; *$p < 0.05$; **$p < 0.01$; ***$p < 0.001$; ****$p < 0.0001$.

ACKNOWLEDGMENTS

We are grateful to K. Kozminski, K. Tanaka, S. Martin, P. Pryciak, E. Bi, D. Lew, T. Davis, R. Tabtiang, and I. Herskowitz for providing strains and plasmids. This work was supported by a research grant (R01-GM114582) from the National Institutes of Health/National Institute of General Medical Sciences. K.E.M. has been supported by the Seilhamer Fellowship from The Jeffrey J. Seilhamer Cancer Foundation.

REFERENCES

Arkowitz RA, Lowe N (1997). A small conserved domain in the yeast Spa2p is necessary and sufficient for its polarized localization. J Cell Biol 138, 17–36.

Bendezu FO, Vincenzetti V, Vavylonis D, Wyss R, Vogel H, Martin SG (2015). Spontaneous Cdc42 polarization independent of GDI-mediated extraction and actin-based trafficking. PLoS Biol 13, e1002097.

Benton BK, Tinkelenberg A, Gonzalez I, Cross FR (1997). Cla4p, a *Saccharomyces cerevisiae* Cdc42p-activated kinase involved in cytokinesis, is activated at mitosis. Mol Cell Biol 17, 5067–5076.

Bi E, Chiavetta JB, Chen H, Chen GC, Chan CS, Pringle JR (2000). Identification of novel, evolutionarily conserved Cdc42p-interacting proteins and of redundant pathways linking Cdc24p and Cdc42p to actin polarization in yeast. Mol Biol Cell 11, 773–793.

Bi E, Park H-O (2012). Cell polarization and cytokinesis in budding yeast. Genetics 191, 347–387.

Brown JL, Jaquenoud M, Gulli MP, Chant J, Peter M (1997). Novel Cdc42-binding proteins Gic1 and Gic2 control cell polarity in yeast. Genes Dev 11, 2972–2982.

Chen GC, Kim YJ, Chan CS (1997). The Cdc42 GTPase-associated proteins Gic1 and Gic2 are required for polarized cell growth in *Saccharomyces cerevisiae*. Genes Dev 11, 2958–2971.

Coffman VC, Nile AH, Lee I-J, Liu H, Wu J-Q (2009). Roles of formin nodes and myosin motor activity in Mid1p-dependent contractile-ring assembly during fission yeast cytokinesis. Mol Biol Cell 20, 5195–5210.

Cvrckova F, De Virgilio C, Manser E, Pringle JR, Nasmyth K (1995). Ste20-like protein kinases are required for normal localization of cell growth and for cytokinesis in budding yeast. Genes Dev 9, 1817–1830.

Di Talia S, Skotheim JM, Bean JM, Siggia ED, Cross FR (2007). The effects of molecular noise and size control on variability in the budding yeast cell cycle. Nature 448, 947–951.

Freisinger T, Klunder B, Johnson J, Muller N, Pichler G, Beck G, Costanzo M, Boone C, Cerione RA, Frey E, Wedlich-Soldner R (2013). Establishment of a robust single axis of cell polarity by coupling multiple positive feedback loops. Nat Commun 4, 1807.

Gandhi M, Goode BL, Chan CS (2006). Four novel suppressors of *gic1 gic2* and their roles in cytokinesis and polarized cell growth in *Saccharomyces cerevisiae*. Genetics 174, 665–678.

Gao XD, Sperber LM, Kane SA, Tong Z, Tong AH, Boone C, Bi E (2007). Sequential and distinct roles of the cadherin domain-containing protein Axl2p in cell polarization in yeast cell cycle. Mol Biol Cell 18, 2542–2560.

Gelperin DM, White MA, Wilkinson ML, Kon Y, Kung LA, Wise KJ, Lopez-Hoyo N, Jiang L, Piccirillo S, Yu H, *et al.* (2005). Biochemical and genetic analysis of the yeast proteome with a movable ORF collection. Genes Dev 19, 2816–2826.

Gladfelter AS, Bose I, Zyla TR, Bardes ESG, Lew DJ (2002). Septin ring assembly involves cycles of GTP loading and hydrolysis by Cdc42p. J Cell Biol 156, 315–326.

Goryachev AB, Leda M (2017). Many roads to symmetry breaking: molecular mechanisms and theoretical models of yeast cell polarity. Mol Biol Cell 28, 370–380.

Guthrie C, Fink GR (1991). Guide to Yeast Genetics and Molecular Biology, San Diego, CA: Academic Press, 194.

Höfken T, Schiebel E (2004). Novel regulation of mitotic exit by the Cdc42 effectors Gic1 and Gic2. J Cell Biol 164, 219–231.

Holden JL, Nur-E-Kamal MSA, Fabri L, Nice E, Hammacher A, Maruta H (1991). Rsr1 and Rap1 GTPases are activated by the same GTPase-activating protein and require threonine 65 for their activation. J Biol Chem 266, 16992–16995.

Iwase M, Luo J, Nagaraj S, Longtine M, Kim HB, Haarer BK, Caruso C, Tong Z, Pringle JR, Bi E (2006). Role of a Cdc42p effector pathway in recruitment of the yeast septins to the presumptive bud site. Mol Biol Cell 17, 1110–1125.

Jaquenoud M, Peter M (2000). Gic2p may link activated Cdc42p to components involved in actin polarization, including Bni1p and Bud6p (Aip3p). Mol Cell Biol 20, 6244–6258.

Jose M, Tollis S, Nair D, Sibarita JB, McCusker D (2013). Robust polarity establishment occurs via an endocytosis-based cortical corralling mechanism. J Cell Biol 200, 407–418.

Kang PJ, Angerman E, Nakashima K, Pringle JR, Park H-O (2004). Interactions among Rax1p, Rax2p, Bud8p, and Bud9p in marking cortical sites for bipolar bud-site selection in yeast. Mol Biol Cell 15, 5145–5157.

Kang PJ, Beven L, Hariharan S, Park H-O (2010). The Rsr1/Bud1 GTPase interacts with itself and the Cdc42 GTPase during bud-site selection and polarity establishment in budding yeast. Mol Biol Cell 21, 3007–3016.

Kang PJ, Lee ME, Park H-O (2014). Bud3 activates Cdc42 to establish a proper growth site in budding yeast. J Cell Biol 206, 19–28.

Kawasaki R, Fujimura-Kamada K, Toi H, Kato H, Tanaka K (2003). The upstream regulator, Rsr1p, and downstream effector, Gic1p and Gic2p, of the Cdc42p small GTPase coordinately regulate initiation of budding in *Saccharomyces cerevisiae*. Genes Cells 8, 235–250.

Klunder B, Freisinger T, Wedlich-Soldner R, Frey E (2013). GDI-mediated cell polarization in yeast provides precise spatial and temporal control of Cdc42 signaling. PLoS Comput Biol 9, e1003396.

Kozminski KG, Beven L, Angerman E, Tong AHY, Boone C, Park H-O (2003). Interaction between a Ras and a Rho GTPase couples selection of a growth site to the development of cell polarity in yeast. Mol Biol Cell 14, 4958–4970.

Kozminski KG, Chen AJ, Rodal AA, Drubin DG (2000). Functions and functional domains of the GTPase Cdc42p. Mol Biol Cell 11, 339–354.

Kozubowski L, Saito K, Johnson JM, Howell AS, Zyla TR, Lew DJ (2008). Symmetry-breaking polarization driven by a Cdc42p GEF-PAK complex. Curr Biol 18, 1719–1726.

Layton AT, Savage NS, Howell AS, Carroll SY, Drubin DG, Lew DJ (2011). Modeling vesicle traffic reveals unexpected consequences for Cdc42p-mediated polarity establishment. Curr Biol 21, 184–194.

Lee ME, Lo WC, Miller KE, Chou CS, Park H-O (2015). Regulation of Cdc42 polarization by the Rsr1 GTPase and Rga1, a Cdc42 GTPase-activating protein, in budding yeast. J Cell Sci 128, 2106–2117.

Marco E, Wedlich-Soldner R, Li R, Altschuler SJ, Wu LF (2007). Endocytosis optimizes the dynamic localization of membrane proteins that regulate cortical polarity. Cell 129, 411–422.

Martin SG (2015). Spontaneous cell polarization: feedback control of Cdc42 GTPase breaks cellular symmetry. Bioessays 37, 1193–1201.

Miller KE, Lo WC, Lee ME, Kang PJ, Park H-O (2017). Fine-tuning the orientation of the polarity axis by Rga1, a Cdc42 GTPase-activating protein. Mol Biol Cell 28, 3773–3788.

Nern A, Arkowitz RA (2000). Nucleocytoplasmic shuttling of the Cdc42p exchange factor Cdc24p. J Cell Biol 148, 1115–1122.

Okada S, Leda M, Hanna J, Savage NS, Bi E, Goryachev AB (2013). Daughter cell identity emerges from the interplay of Cdc42, septins, and exocytosis. Dev Cell 26, 148–161.

Okada S, Lee ME, Bi E, Park H-O (2017). Probing Cdc42 polarization dynamics in budding yeast using a biosensor. Methods Enzymol 589, 171–190.

Orlando K, Zhang J, Zhang X, Yue P, Chiang T, Bi E, Guo W (2008). Regulation of Gic2 localization and function by phosphatidylinositol 4,5-bisphosphate during the establishment of cell polarity in budding yeast. J Biol Chem 283, 14205–14212.

Ozbudak EM, Becskei A, van Oudenaarden A (2005). A system of counteracting feedback loops regulates Cdc42p activity during spontaneous cell polarization. Dev Cell 9, 565–571.

Park H-O, Bi E, Pringle JR, Herskowitz I (1997). Two active states of the Ras-related Bud1/Rsr1 protein bind to different effectors to determine yeast cell polarity. Proc Natl Acad Sci USA 94, 4463–4468.

Rapali P, Mitteau R, Braun C, Massoni-Laporte A, Unlu C, Bataille L, Arramon FS, Gygi SP, McCusker D (2017). Scaffold-mediated gating of Cdc42 signalling flux. eLife 6, 25257.
Rida CG, Surana U (2005). Cdc42-dependent localization of polarisome component Spa2 to the incipient bud site is independent of the GDP/GTP exchange factor Cdc24. Eur J Cell Biol 84, 939–949.
Roemer T, Madden K, Chang J, Snyder M (1996). Selection of axial growth sites in yeast requires Axl2p, a novel plasma membrane glycoprotein. Genes Dev 10, 777–793.
Sadian Y, Gatsogiannis C, Patasi C, Hofnagel O, Goody RS, Farkasovsky M, Raunser S (2013). The role of Cdc42 and Gic1 in the regulation of septin filament formation and dissociation. eLife 2, e01085.
Shimada Y, Gulli M-P, Peter M (2000). Nuclear sequestration of the exchange factor Cdc24p by Far1 regulates cell polarity during mating. Nat Cell Biol 2, 117–124.
Slaughter BD, Das A, Schwartz JW, Rubinstein B, Li R (2009). Dual modes of cdc42 recycling fine-tune polarized morphogenesis. Dev Cell 17, 823–835.
Slaughter BD, Unruh JR, Das A, Smith SE, Rubinstein B, Li R (2013). Non-uniform membrane diffusion enables steady-state cell polarization via vesicular trafficking. Nat Commun 4, 1380.
Smith SE, Rubinstein B, Mendes Pinto I, Slaughter BD, Unruh JR, Li R (2013). Independence of symmetry breaking on Bem1-mediated autocatalytic activation of Cdc42. J Cell Biol 202, 1091–1106.
Snyder M (1989). The SPA2 protein of yeast localizes to sites of cell growth. J Cell Biol 108, 1419–1429.
Snyder M, Gehrung S, Page BD (1991). Studies concerning the temporal and genetic control of cell polarity in *Saccharomyces cerevisiae*. J Cell Biol 114, 515–532.
Takahashi S, Pryciak PM (2007). Identification of novel membrane-binding domains in multiple yeast Cdc42 effectors. Mol Biol Cell 18, 4945–4956.
Toenjes KA, Sawyer MM, Johnson DI (1999). The guanine-nucleotide-exchange factor Cdc24p is targeted to the nucleus and polarized growth sites. Curr Biol 9, 1183–1186.
Tong Z, Gao XD, Howell AS, Bose I, Lew DJ, Bi E (2007). Adjacent positioning of cellular structures enabled by a Cdc42 GTPase-activating protein-mediated zone of inhibition. J Cell Biol 179, 1375–1384.
Witte K, Strickland D, Glotzer M (2017). Cell cycle entry triggers a switch between two modes of Cdc42 activation during yeast polarization. eLife 6, 26722.
Woods B, Lai H, Wu CF, Zyla TR, Savage NS, Lew DJ (2016). Parallel Actin-Independent Recycling Pathways Polarize Cdc42 in Budding Yeast. Curr Biol 26, 2114–2126.
Zheng Y, Bender A, Cerione RA (1995). Interactions among proteins involved in bud-site selection and bud-site assembly in *Saccharomyces cerevisiae*. J Biol Chem 270, 626–630.